Journal of Thermal Analysis and Calorimetry, Vol. 80 (2005) 739–747

CALORIMETRIC ANALYSIS OF AM60 MAGNESIUM ALLOY

P. Bassani[1*], *E. Gariboldi*[2] *and A. Tuissi*[1]

[1]CNR-IENI, Lecco C.so Promessi Sposi 29, 23900 LC, Italy
[2]Politecnico di Milano, Department of Mechanics, via La Masa 34, 20156 Milano, Italy

Calorimetric analysis is commonly used for the study of several solid state transformations, among which phase transformations. Information about enthalpy, kinetics and general features of transformations could be obtained with suitable configurations of the analysis equipment and arrangements of the tests procedures. An experimental analysis of the transformations occurring in a Mg–Al–Mn alloy, namely AM60, has been performed on samples cut from as die-cast components. The results obtained confirmed that calorimetric analysis is a suitable method for the study of transformations of such kind of alloys. Using the technique of multiple heating rate tests, an estimation of activation energy of dissolution of $Mg_{17}Al_{12}$ phase has been derived.

Keywords: *DSC, magnesium alloy AM60, phase transformation kinetics*

Introduction

Magnesium alloys, especially magnesium-aluminium alloys are often used for vehicle applications due to their combination of good ductility and tensile properties. Generally near net shape parts can be produced by die-casting techniques. As a result of the high cooling rate experienced by the material that solidifies in a steel-die, the microstructure is characterized by the presence of non-equilibrium structures [1]. When the principal alloying element is aluminium, the main phases encountered are magnesium solid solution (α-phase) both as homogeneous grains and separated by a divorced eutectic structure, formed together with the brittle $Mg_{17}Al_{12}$ intermetallic phase [2]. Thermal treatments are sometimes performed in order to modify this microstructure, and to achieve increased stability to medium service temperature. It is useful to remind that maximum service temperature for such magnesium alloys is of about 120°C, that correspond to about 0.4–0.5T_m, a rather high homologous temperature [3]. In order to predict adequately the effect of thermal treating or of maintenance at high temperature on the alloy properties, a better understanding of the kinetic aspects of the transformations occurring is needed.

Calorimetric techniques are widely used for several thermodynamic evaluation of chemical and physical reactions, mainly of inorganic and organics materials [4]. In the field of metallurgy, several authors have used calorimetric techniques for the evaluation of precipitation processes [5–8], recrystallization [9, 10], phase transformation [11–14], and even for deriving CCT diagrams [15]. From isothermal or non-isothermal calorimetric experiments also kinetic features of the transformations, such as Arrhenius parameters and reaction model, could be obtained. Several methods for the analysis of experimental data have been proposed in literature, as outlined in reviews of the matter [6, 12, 16]. Among them, isoconversional methods are known as the most reliable, as they allow for evaluating Arrhenius parameters independently from the reaction model adopted [4, 17–20].

The aim of the present work was to check the suitability of calorimetric investigations on the microstructural modifications brought about by thermal cycles on as die-cast magnesium alloys. DSC analyses were combined with SEM observations and EDS microanalyses in order to define the transformations involved and their kinetics. Among several methods found in literature, the isoconversional Kissinger method [17, 21] has been used to estimate the kinetic of dissolution of non-equilibrium phases.

Experimental

The alloy used in this investigation is an AM60 magnesium alloy, the nominal and actual compositions of which are reported in Table 1. The material was received as 3 mm thick plate, produced by cold-chamber high pressure die-casting technique. The alloy was investigated in the as-cast microstructural condition (AC), here presented in Fig. 1. The as received material was analysed by optical and scanning electron microscopy.

AM60 was selected as test material due to its relatively simple metallurgy. The main alloying ele-

* Author for correspondence: paola.bassani@ieni.cnr.it

1388–6150/$20.00

Akadémiai Kiadó, Budapest, Hungary
Springer, Dordrecht, The Netherlands

Table 1 Nominal composition (mass%) of AM60 alloy and of the investigated plates

	Alloy elements/mass%								
	Al	Mn	Si	Zn	Fe	Cu	Ni	Others	Mg
Nominal	5.5–6.5	0.25	0.1	0.22	0.005	0.01	0.002	0.003	BAL.
Test material	5.85	0.25	0.003	0.0029	–	–	–	–	BAL.

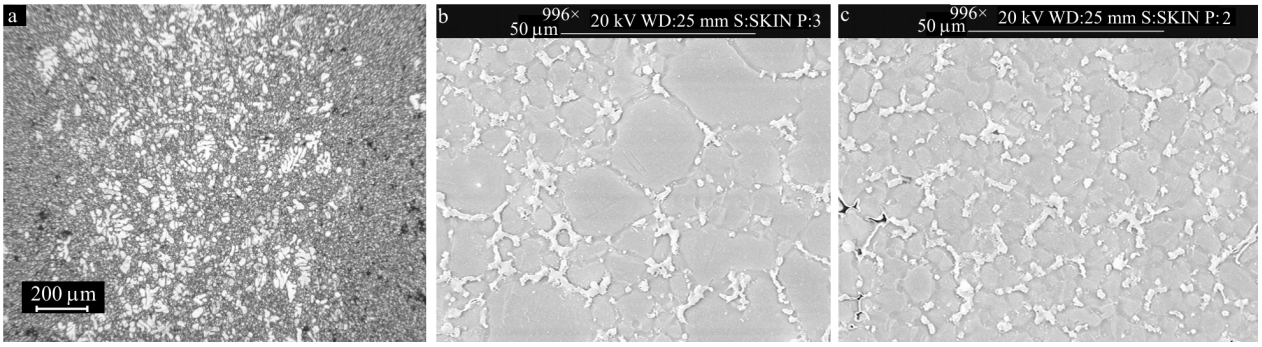

Fig. 1 a – Light optical image of a transversal section of an AM60 plate in the as die-cast condition; b, c – scanning electron micrographs of AM60 alloy, in a central region and skin layer, respectively. Eutectic structure made of $Mg_{17}Al_{12}$ and Al-rich Mg solid solution can be clearly seen in interdendritic spaces. Bright globular AlMn(Fe) particles are also visible

ments are aluminium and, in low amount, manganese. The latter element is mainly added to improve the corrosion resistance of the alloy. Mn is mainly combined with aluminium and iron in the high-melting AlMn(Fe) particles. Such phases are virtually insensitive to thermal treatment and thus the Mg–Al binary diagram (Fig. 2 [22]) can be used as a basis for the understanding of the behaviour of this alloy.

The general microstructure revealed the presence of dendrite branches of solid solution of Al in Mg (α-phase) and divorced eutectic structure made of Al-rich Mg solid solution and $Mg_{17}Al_{12}$ (β-phase) (Fig. 1). Moreover, globular particles of AlMn(Fe), mainly located at interdendritic spaces, were observed. This macrostructure revealed a sandwich structure, made up of an inner layer, characterized by a coarse structure, between two skin layers, which displayed a finer microstructure. In the present samples the skin layer extended for about 1 mm below the external surfaces, and in the examined thin specimens it covered more than 60% of the total volume. Further, the skin layer was relatively free of the so-called floating crystals, the large dendrites that were rather frequent in the inner layer (Fig. 1a). Floating crystals nucleated in the shot sleeve prior to be injected into the mould, in a region where material dis-homogeneity frequently occurs. Occasionally porosity was found in the boundary zone between skin and core. The defect as well as the other microstructural features are typically found in thin high-pressure die-cast components made of Mg alloys [1].

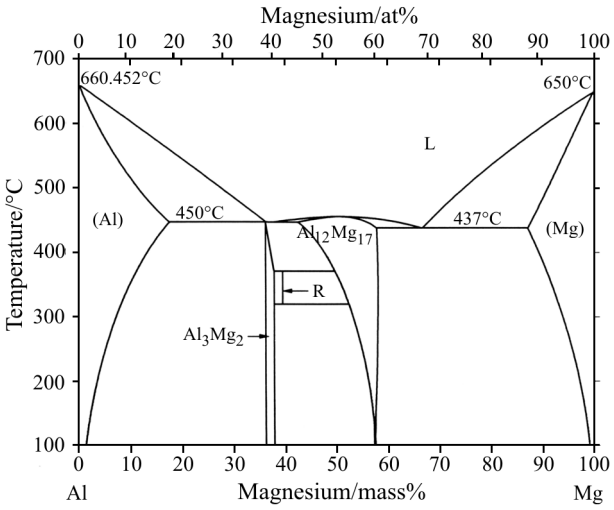

Fig. 2 Mg–Al binary phase diagram. AM60 alloy is placed in the Mg rich part of the diagram and Al content is intermediate between minimum and maximum solubility content in Mg matrix. After Massalsky [22]

Specimens were cut from the plate using a metallographic diamond cutting saw. They were then ground to final shape with emery papers. Final mass of each sample was of about 50 mg. Tests were performed with a Setaram Labsys TG-DTA system, equipped with a detector configured for DSC analysis in a temperature range from room temperature (RT) up to 800°C. Temperature and heat flow calibration was performed using pure indium and tin melting points. The heating chamber was fluxed with nitrogen. When testing AM60 alloy, sample mass was checked before and after DSC runs using a high accuracy balance. No significant increase of the mass was observed, even when a slight oxidation of the sample surfaces was visually observed.

A first set of thermal scans was performed by heating the samples from RT to 550°C at different

heating rates (ϕ), and cooling them at a fixed rate (10 K min^{-1}). The aim of such tests was to check the sensitivity of the reactions to the heating rate. A second set of scans was performed at fixed heating and cooling rates (30 and 20 K min^{-1}, respectively) from RT to different maximum temperatures of 450, 475, 500 and 550°C. This set of tests was designed to confirm the presence of eutectic structure melting and to check the stability of the melt during the subsequent overheating.

Additional tests were performed with a Seiko Instruments DSC 220, an instrument with similar operational range but different building characteristics, in which the tests could be interrupted once the maximum temperature was reached and the sample quickly air cooled, in order to freeze the microstructure.

A sample for each scan cycle as well as the as-cast material were polished with conventional metallographic techniques. After etching with acetic picral (a mixture of ethanol, picric acid, acetic acid and water), the samples were observed by light optical microscopy (OM) and scanning electron microscopy (SEM). EDXS (energy dispersion X-ray spectrometry) measurements of composition were also performed to check the occurrence and evaluate the degree of thermal homogenization effects.

Results

DSC analysis

Representative DSC curves from the first set of tests at different heating rate are shown in Fig. 3. Four anomalies can be identified. As can be clearly seen all scans show a wide peak ranging from about 300 to 450°C (clearly shown in Fig. 3a and hereafter referred as peak 2). Other two peaks, more evident in high scan rate tests, can be observed: a large and smooth peak at about 150°C (peak 1), and small and sharp peak at about 440°C (peak 3). At higher temperature, a significant endothermic deviation of the heat flow curves can be appreciated just before the maximum temperature. This anomaly can be interpreted as the onset of a large peak (peak 4).

All cooling curves generally showed no significant peak. In some case in the first set of tests that was carried out, a peak was detected at high temperature. The occurrence of this peak was associated to a perturbation of TG signal. These effects were then attributed to the occurrence of oxidation phenomena. The following metallographic inspection of such samples showed the presence of a great concentration of oxides and a high presence of interconnected shrinkage porosity, localized in the skin layer of some regions of the die-cast material. In such porosity residuals of cleaning substances (such as water or ethylic alcohol)

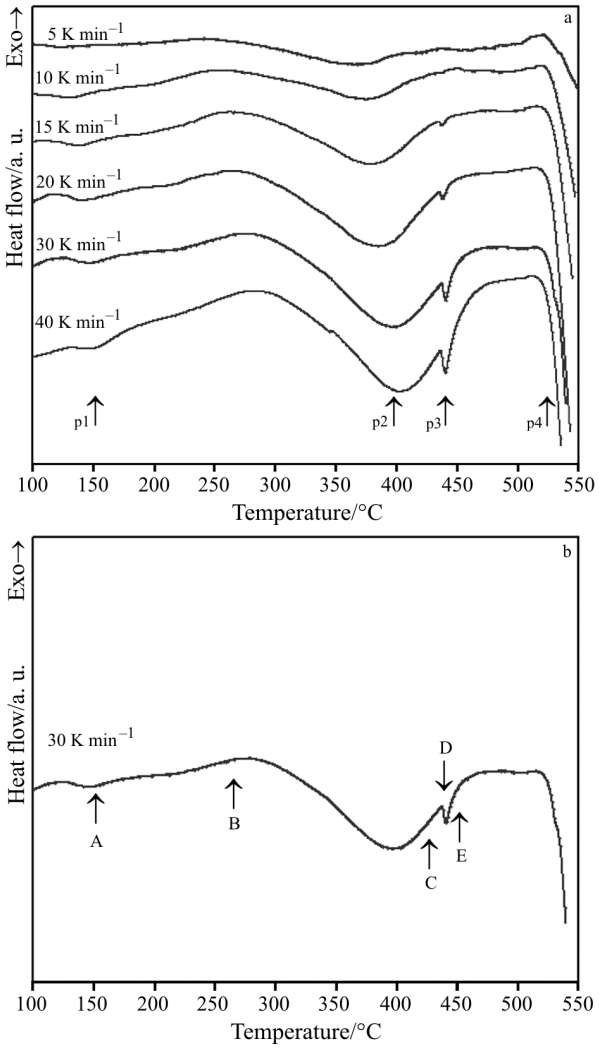

Fig. 3 a – DSC scans of AM60 magnesium alloy performed at different heating rates. An evolution of the shape of the curve can be clearly observed; b – DSC scan at 30 K min^{-1} with arrows showing the interruption temperatures of samples that were subsequently air quenched

were retained by capillarity effects and provided the necessary oxidizing agent. Longer cleaning cycles before thermal scans prevented oxidation in the following sets of specimens.

Each peak was characterized by initial (T_0), peak (T_p), end (T_e) temperatures and heat content (ΔH), although it was not possible to determine all these parameters with the same accuracy. The peak temperature was well assessed for all peaks, with the exception of peak 4 for obvious reasons, while the initial and end temperature data of peaks 1 and 2 were widely scattered due to the smooth and broad nature of the peaks and to the curved baseline. The uncertainty also affected reaction heats evaluation of these peaks. Peak 3 was sharp, when present, but it was overlapped to peak 2. For this reason, also the data referring to peak 3

Table 2 Mean values obtained by analysis from DSC peaks of scans at different heating rates

Heating rate	Peak 1		Peak 2		Peak 3		Peak 4	
ϕ/K min^{-1}	T_p/°C	ΔH/J g^{-1}	T_p/°C	ΔH/J g^{-1}	T_0/°C	T_p/°C	ΔH/J g^{-1}	T_0/°C
5	125.12	6.5	364.0	10.2	–	422	–	528.0
10	133.00	4.2	375.0	9.4	435.5	438	0.014	528.0
15	140.20	1.8	381.0	10.5	435.8	439	0.044	529.0
20	145.00	1.9	386.5	11.6	436.0	439	0.072	527.5
30	149.81	1.5	393.0	9.8	436.9	441	0.096	527.0
40	152.20	0.3	402.0	10.4	437.6	442	0.169	526.0

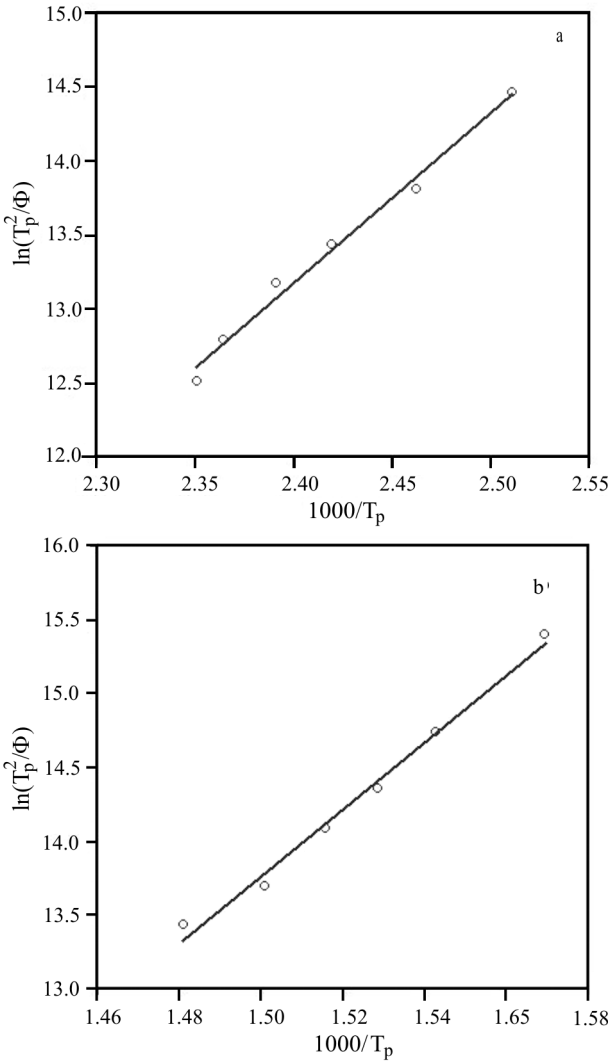

Fig. 4 Kissinger plots: $\ln(T_p^2/\phi)$ *vs.* $1/T_p$, where T_p is the peak temperature and ϕ is the heating rate; a – peak 1, b – peak 2

were affected by a slight uncertainty. An improved estimation of temperatures and heat contents for peak 3 would require convolution of peaks 2 and 3.

The above data are summarised in Table 2.The kinetic analysis peaks was performed by isoconversional Kissinger analysis, starting from the fundamental kinetic Eq. (1),

$$d\alpha/dt=k(T)f(\alpha) \quad (1)$$

where t, α, $k(T)$, $f(\alpha)$ are time, extent of conversion, rate constant, reaction model, respectively. $k(T)$ is generally replaced by the Arrhenius equation:

$$k(T)=A\exp(-E/RT) \quad (2)$$

where A, E, R are Arrhenius pre-exponential factor, activation energy, gas constant in the order.

In the case of constant heating rate tests, the following relation can be derived:

$$\ln(T_p^2/\phi)+E/RT_P=\text{constant} \quad (3)$$

where ϕ, T_P are heating rate expressed as K s^{-1}, and peak temperature, respectively. E was obtained by plotting $\ln(T_p^2/\phi)$ *vs.* $1/T$. Values obtained for peaks 1 and 2 are reported in Table 3, while the corresponding fitting curves are reported in Figs 4a and b.

A similar procedure was applied for peak 2 considering the temperature T_α corresponding to a fixed extent of conversion (α) ranging from 0.3 to 0.7, instead of T_p. This procedure was used in order to check possible variations of activation energy over the broad temperature range for the transformation corresponding to peak 2. Good agreement with mean values were obtained. The results are summarised in Table 3, which also lists the parameter r. This parameter is an index describing the quality of the fitting, based on normalized residuals from regression procedure: if r=1, the experimental data lie on a single line.

After numerical derivation of $d\alpha/dt$, using E values obtained from Kissinger analysis, an attempt to describe the calculated numerical $f(\alpha)$ for peak 2 in terms of known kinetic functions was attempted. Table 4 summarises three reaction models that were taken into account for the present analysis. The conventional name of the model is presented in the first column and the corresponding $f(\alpha)$ equations are given in the second column. Experimental data were best-fitted giving the values of n and the r-parameter listed in the same table. It was observed that the well-known JKMA equation, adapted for

Table 3 Activation energies obtained from Kissinger analysis of peak data

	Peak 1		Peak 2				
	T_p	T_p	T_α				
			α=0.3	α=0.4	α=0.5	α=0.6	α=0.7
E/kJ mol^{-1}	94±3	185±5	182.3	184.6	186.5	186.8	186.6
r	0.988	0.989	0.987	0.986	0.983	0.978	0.974

Table 4 Set of reaction models applied to peak 2

Model	$f(\alpha)$	n	r
JKMA ($0.5 \le m \le 4$)	$m(1-\alpha)[-\ln(1-\alpha)]^{1-1/m}$	0.36–0.42 0.5 (forced)	0.99 0.89
three-dimensional diffusion	$2(1-\alpha)^{2/3}[1-(1-\alpha)^{1/3}]^{-1}$	–	0.89
power law	$1/\alpha^n$	1.5–1.9	0.99

non-isothermal data [18], give a best fitting only for n values of 0.45–0.35, well below 0.5, the lower limit accepted for n values. This value is similar to that found by Payzant *et al*. [23], through isothermal experiments and Avrami modelling. A model to describe thermal decomposition in solids based on 3-dimensional diffusion reported by Vyazovkin and Wight [24] gave similar results. Good fitting was found for a power law with n from 1.5 to 1.9.

Microstructural observations

OM and SEM observations coupled with EDXS analysis were performed on selected specimens after DSC analyses. Samples heated at different heating rates up to 550°C and cooled at the same rate, showed significant homogenization. No appreciable differences were detected apart from occasional slightly coarsened grains. A second cycle at 450°C showed no peak during heating. This confirms the homogenization effect of scans to 550°C.

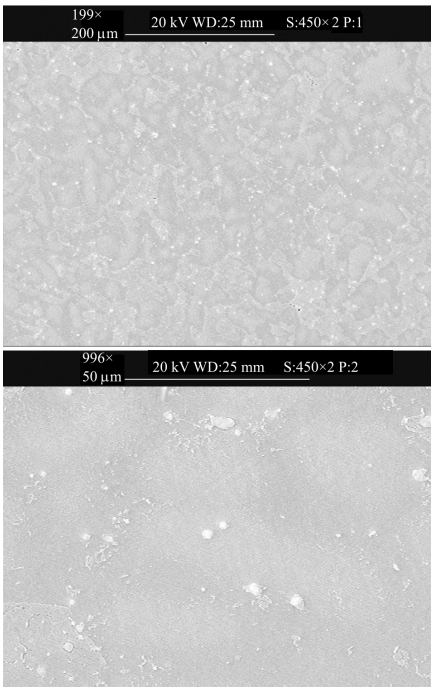

Fig. 5 Specimen heated 2 times up to 450°C at 30 K s^{-1} and cooled at 20 K min^{-1}. Higher magnification image shows continuous precipitation of β-phase of very small size

Although during cooling from 550°C, even at different cooling rates, no peak was detected, SEM observations revealed the occurrence of precipitation phenomena. β particles in Al-rich zones in different amount and size were observed depending on the cooling rate. When the minimum cooling rate was followed, such small particles were also found in the core regions. In any case, the very low amount of this phase could be consistent with the absence of peaks (Figs 5 and 6).

Heating up to different temperatures at the same heating rate in the second set of tests caused the progressive smoothing of coring effects that characterize the as die-cast structure. This was confirmed by sets of microanalyses carried out on the interior of the grains and the grain boundary regions. The mean Al content at the centre of grains is reported in Fig. 7, where small and large grains were considered separately. In the as die-cast condition, the Al content is lower in large grains, that were probably the first solidified regions. As temperature increases the Al content tend to increase both in small and large grains, as a consequence of diffusion phenomena from the Al-rich α-phase at grain boundary. As expected, since the diffusion path is longer in large grains, the increase of Al at their core is slower than that observed in the smallest grains. At about 500°C, due to the existence of macro-inhomogenities, the Al-content at the centre of small grains reached peak values that overcame the average Al content of the alloy. Higher test temperatures were able to reduce macro-heterogenities and the amount of Al at the centre of small and large grains tended to converge to the average value. The distribution of the fine

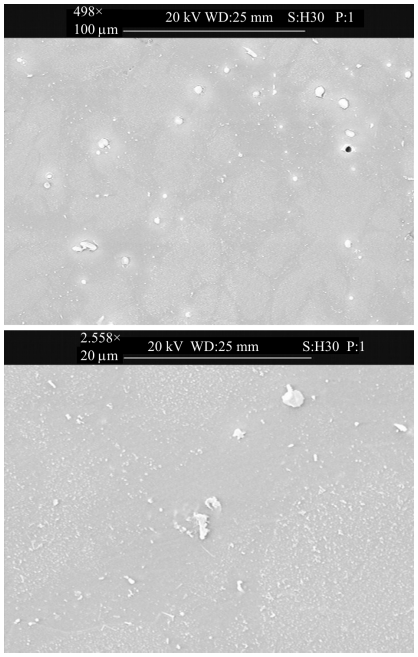

Fig. 6 Microstructural features of specimen heated at 30 K min^{-1} up to 550°C and cooled at 10 K min^{-1}

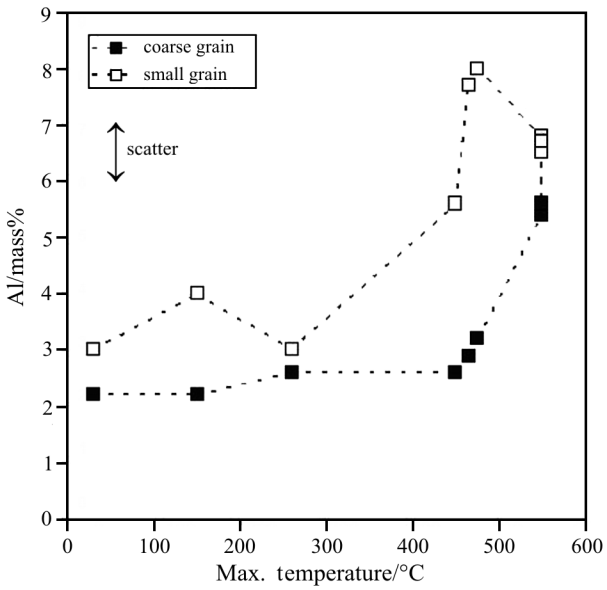

Fig 7 Average Al content at grain centre, for coarse (about 50 µm diameter) and small (about 10 µm diameter) grains of the core layer of samples as a function of maximum temperature reached during heating. Samples have been heated at 30 K min^{-1} and immediately air quenched

β-phase particles (formed during cooling in greater amount in Al-enriched regions) confirmed the modification of the distribution of Al content after cycles up to different temperatures.

In order to clarify the origin of the observed DSC peaks, specimens air-quenched after reaching the maximum temperature were observed. Samples heated up to 150 and 260°C showed no apparent microstructural modification with respect to the specimens cooled in the DSC furnace and to the as die-cast reference samples (Figs 8a, b). Holding at 260°C caused precipitation of fine β phase at grain interiors only in small grains, where the Al content is higher than the maximum solubility of Al in Mg at that temperature (Fig. 8c). To discriminate between these two microstructure TEM analyses could be helpful.

In the thermal cycles that reached the highest temperatures the presence of dissolution of the eutectic structure was witnessed by a peak at 440°C (in Al–Mg phase diagram shows an eutectic line at 437°C). The existence of liquid phase in these samples was confirmed by microstructural observations carried out on specimen air quenched from different temperature, as shown in Fig. 9.

Discussion

During thermal analyses four peaks have been identified. For each peak, on the bases of the results obtained from all the investigations, an explanation of their origin is presented.

Peak 1

The first effect was characterized by a T_p of about 150°C, and by an activation energy of about 90 kJ mol^{-1}, similar to the activation energy of grain boundary diffusional processes in Mg alloys [25]. Earlier study on precipitation kinetics in Al-rich Mg alloys gave activation energy of the order of 40 kcal g-atom^{-1} (138 kJ mol^{-1}) [26], in reasonable agreement with the value found for peak 1 activation energy. No further kinetic analysis was attempted, due to broad and not well defined shape of the peak. OM and SEM analyses did not show any apparent modification of microstructure of the samples quenched after this peak (Fig. 8).

This peak could be related to dissolution of very small precipitate, formed during the last stage of cooling in die-cast mould, or during the first stage of the heating ramps. It is well known that in Mg–Al alloys at increasing Al content precipitation phenomena from solutionized materials occur at lower temperature and with faster kinetics [15, 27]. Even in as cast materials, precipitation could take place if very high supersaturation is present and enough time is provided during cooling from solidification to room temperature. No precipitation DSC signal could be detected at temperatures lower than peak 1 with the employed DSC instrument and it is not possible at present to discriminate between the two hypothesis.

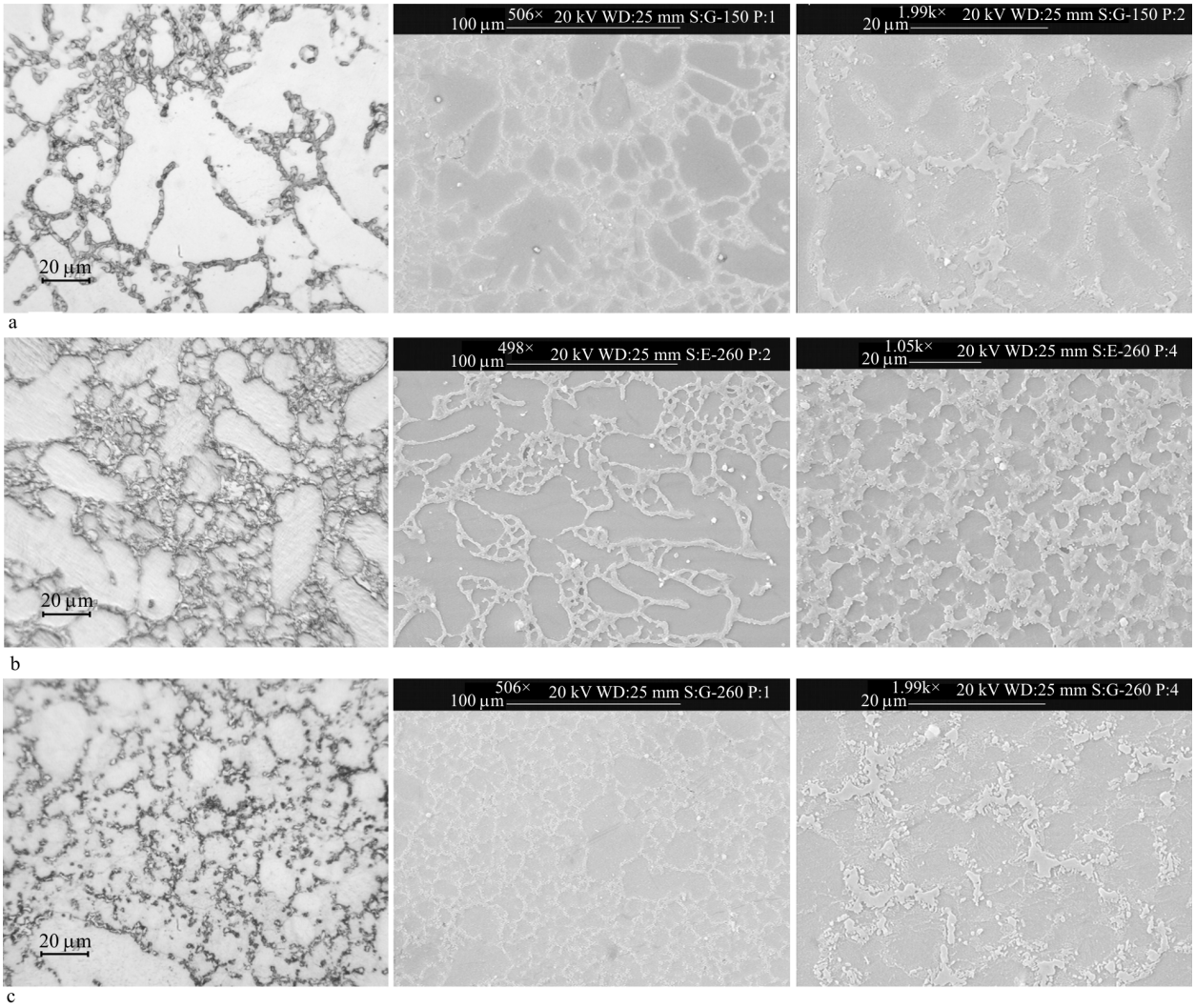

Fig. 8 MO micrographs and SEM micrographs of sample heated up at 30 K min^{-1} to different temperature: a – up to 150°C, then air quenched, (ref. Fig. 3b, sample a); b – up to 260°C and then air quenched (ref. Fig. 3b, sample b); c – up to 260°C, maintained for 3 h and then cooled at 10 K min^{-1}

Peak 2

This second peak, spread over more than 150°C, between 300 and 450°C, can be associated to the dissolution of $Mg_{17}Al_{12}$ and to the redistribution of Al in the Mg matrix: micrographs of Figs 8 and 9 show $Mg_{17}Al_{12}$ disappears. EDS microanalyses (Fig. 7) also confirm the redistribution of Al inside the grains and progressive homogenization of the alloy during heating. Activation energy of this process (about 185 kJ mol^{-1}) seems too high compared to diffusion activation energies in Mg alloy (self-diffusion: 136 kJ mol^{-1}, grain boundary self-diffusion: about 90 kJ mol^{-1}) [25]. Since diffusion alone cannot account for such values, additional effects accounting for the disruption of the ordered structure of $Mg_{17}Al_{12}$ and adjustment of coherency stresses should be invoked. Inhomogeneity, due to strong coring effect in as die-cast material, also can disturb diffusional phenomena and contribute to higher activation energy. Moreover, kinetic analyses showed that this process does not follow a simple JKMA behaviour of nucleation and diffusion, confirming the complexity of the phenomena. A three-dimensional diffusion process with a chemical controlling mechanism can be supposed.

Peak 3

It is a melting peak corresponding to melting of zones where Al content exceeds solid solubility limit (about 12 mass%) having eutectic structure. This fact is supported by several observations. T_0 is very close to 437°C, the eutectic melting temperature from equilibrium Mg–Al diagram. OM micrographs confirmed the presence of formerly molten regions at grain boundary at peak temperatures. By increasing the heating rate, less time is available for diffusional mechanisms and a wider Al-enriched region is present. Correspondingly peak 3 is more visible and its enthalpy is increased.

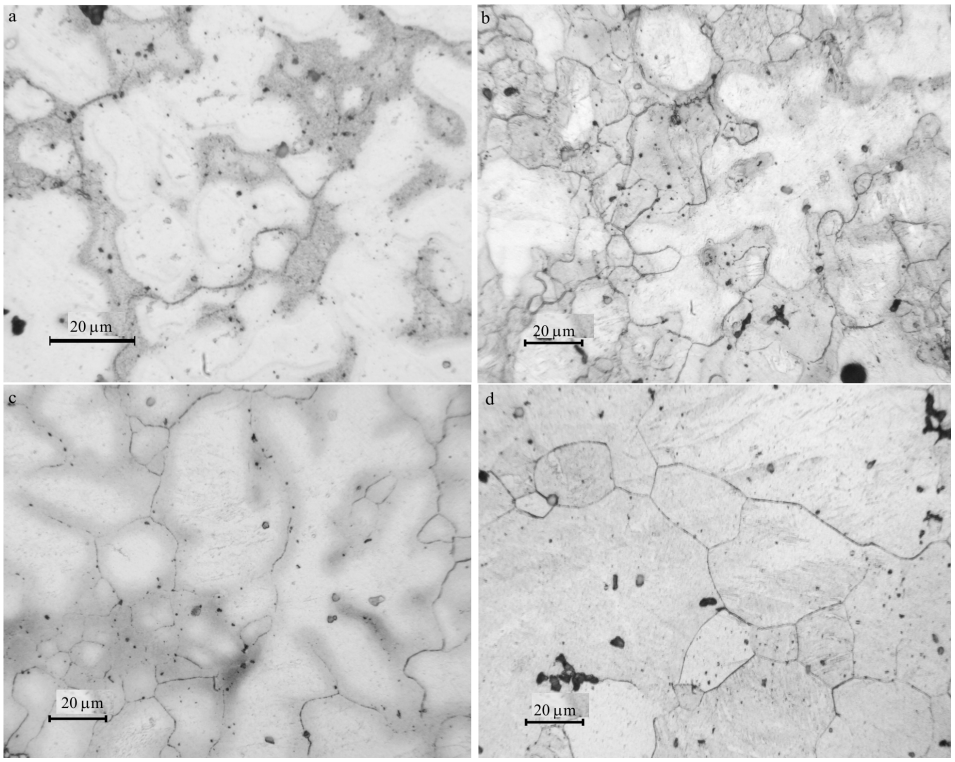

Fig. 9 Samples heated up to peak 3: a – onset of peak, b – peak and c – offset of peak +10°C temperature (ref. Fig. 3b; tests interrupted at points C, D, E respectively), and d – sample heated up to 550°C, and air quenched

Peak 4

Even at slow heating rates, at which the dissolution of $Mg_{17}Al_{12}$ is completed before reaching eutectic temperature and no high Al regions (>11%) remains, still inhomogeneity is present. At grain boundary and also in the centre of small grain regions Al content higher than equilibrium (5.85%) could be found. In the as die-cast alloy these regions of small grains are surrounded by large amount of $Mg_{17}Al_{12}$, increasing local mean Al content. These regions start melting at temperatures as low as 530°C if the Al content exceeds 7 mass%. The onset temperature seems to decrease with increasing heating rate, even if increasing ϕ generally causes peak temperatures to increase. At higher heating rate less time is available for homogenization of the alloy, therefore, the Al content of Al-rich regions is higher and the corresponding incipient melting temperature is lower. This is also confirmed by results gathered on samples heated twice at maximum temperature. The analyses showed negligible or no inhomogeneities, and DSC scans showed the absence of the fourth peak. Incipient melting temperature for solutionized Mg–Al alloy with nominal Al content of 5.85% is in fact higher than 550°C.

Conclusions

Calorimetric investigations were used for the analysis of dissolution/precipitation phenomena occurring in as die-cast AM60 magnesium alloy.

Two main endothermic effects related to the presence of precipitates and unstable phases were found during controlled heating of the AM60 alloy. These effects could be related to dissolution phenomena of unstable phases. The first effect was characterized by a T_p of about 150°C, and by an activation energy of about 90 kJ mol^{-1}, similar to activation energy of grain boundary or pipe diffusion processes in Mg alloys. As OM and SEM analyses did not show any apparent modification of microstructure, this peak was related to dissolution of very small precipitates. The second main effect was characterized by a T_p of about 390°C and activation energy of about 185 kJ mol^{-1}. This second peak is related to dissolution of the $Mg_{17}Al_{12}$ phase.

At higher heating rate, a third endothermic peak could be detected that could be ascribed to local melting of Al enriched regions, corresponding to the eutectic structure. The low sensitivity of this peak to heating rate, the onset temperature, very close to eutectic temperature, and metallographic evidences in quenched samples of melting at grain boundary supported this thesis.

Finally the onset of a fourth endothermic peak could be identified. This peak corresponded to the on-

set of melting processes of Al rich-zones, in limited regions of chemically inhomogeneous alloy.

Further investigations are needed to clarify dissolution phenomena and the exact mechanisms lying at the bases of the two main dissolution processes depicted above. Activation energies obtained through DSC analysis are experimental bases on which develop future work.

Acknowledgements

The authors would like to thank Meridian-Magnesium Products of Italy for supplying magnesium alloy.

References

1 A. K. Dahle, Y. C. Lee, M. D. Nave, P. L. Schaffer and D. H. StJohn, J. Light Met., 1 (2001) 61.
2 D. J. Sakkimem, Physical Metallurgy of Magnesium Die-Cast alloys, SAE Paper 946779, Ed. SAE, Detroit USA 1999.
3 T. K. Aume and H. Westgmgen, Property update of Magnesium Die-casting Alloys, SAE PAPER 950424, SAE, Detroit USA 1997.
4 T. Ozawa, Thermochim. Acta, 355 (2000) 35.
5 M. Nicolas and A. Deschamps, Metall. Mater. Trans. A, 35 (2004) 1437.
6 G. Biroli, G. Caglioti, L. Martini and G. Riontino, Scripta Mater., 39 (1998) 197.
7 S. Abis, M. Massazza, P. Menegucci and G. Riontino, Scripta Mater., 45 (2001) 685.
8 S. Abis, P. Menegucci and G. Riontino, Philos. Mag. B, 67, p. 465.
9 C. E. Rodrìguez Torres, F. H. Sànchez, A. Gonzàlez, F. Actis and R. Herrera, Metall. Mater. Trans. A, 33 (2002) 25.
10 K. Chrissafis, K. G. Efthimiadis, E. K. Polychroniadis and S. C. Chadjivasiliou, J. Therm. Anal. Cal., 74 (2003) 761.
11 L. Battezzati, M. Baricco, F. Marongiu, G. Serramoglia and D. Bergesio, Metall. Sci. Tech., 19, pp. 16–20.
12 G. Riontino and S. Abis, Philos. Mag. B, 64 (1991) 447.
13 V. Vassilev, L. Aljihmani and V. Paranova, J. Therm. Anal. Cal., 76 (2004) 727.
14 M. Gojic, M. Suceska and M. Rajic, J. Therm. Anal. Cal., 75 (2004) 947.
15 G. V. Raynor, The physical metallurgy of magnesium and its alloys, Pergamon Press, London 1959, pp. 343–348.
16 H. Tanaka, Thermochim. Acta, 267 (1995) 29.
17 M. J. Starink, Thermochim. Acta, 404 (2003) 163.
18 J. Baram and V. Erukhimovitch, Thermochim. Acta, 291 (1997) 81.
19 J. Baram and V. Erukhimovitch, Thermochim. Acta, 323 (1998) 43.
20 S. Vyazovkin, Thermochim. Acta, 355 (2000) 155.
21 G. W. Smith, W. J. Baxter and R. K. Mishra, J. Mater. Sci., 35 (2000) 3871.
22 B. Massalski, Binary Alloy Phase Diagrams - Second Edition, ASM International, Materials Park, Ohio.
23 E. A. Payzant, S. R. Agnew, Q. Han and S. Viswanathan, '$Mg_{17}Al_{12}$ phase precipitation kinetics in die casting alloys AZ91D and AM60B', Magnesium Technology - 2001 TMS Annual Meeting, New Orleans, LA, USA, 11–15 Feb 2001, pp. 183–187.
24 S. Vyazovkin and C.A. Wight, Thermochim. Acta, 340–341 (1999) 53.
25 H. J. Frost and M. F. Ashby, Deformation-mechanism maps, Pergamon Press, Oxford UK 1982.
26 C. Sheldon Roberts, Magnesium and its Alloys, Wiley and Sons, New York 1960, p. 122.
27 Q. M. Amir and S. P. Gupta, Can. Metall. Q., 34 (1995) 43.